A comparative kinetic study of C8–C10 linear alkylbenzenes pyrolysis in a single-pulse shock tube

Wenyu Sun, Alaa Hamadi, Said Abid, Nabiha Chaumeix, Andrea Comandini

Combustion and Flame 221 (2020) 136–149

Contents lists available at ScienceDirect

Combustion and Flame

journal homepage: www.elsevier.com/locate/combustflame

A comparative kinetic study of C_8–C_{10} linear alkylbenzenes pyrolysis in a single-pulse shock tube

Wenyu Sun[a,*], Alaa Hamadi[a], Said Abid[a,b], Nabiha Chaumeix[a], Andrea Comandini[a,*]

[a] CNRS-INSIS, I.C.A.R.E., 1C, Avenue de la recherche scientifique, 45071 Orléans cedex 2, France
[b] Université d'Orléans, 6 Avenue du Parc Floral, 45100 Orléans, France

ARTICLE INFO

Article history:
Received 8 June 2020
Revised 21 July 2020
Accepted 21 July 2020

Keywords:
Ethylbenzene
n-propylbenzene
n-butylbenzene
Single-pulse shock tube
Polycyclic aromatic hydrocarbon (PAH)

ABSTRACT

This work presents a comparative study on the pyrolysis of C_8–C_{10} linear alkylbenzenes including ethylbenzene, *n*-propylbenzene and *n*-butylbenzene. Experiments were performed with highly diluted mixtures in argon containing respectively the three fuels under nearly identical conditions in a single-pulse shock tube, at a nominal pressure of 20 bar and over a temperature range of 950–1700 K. Post-shock gas mixtures were sampled and analyzed with the gas chromatographic technique so that species concentration evolutions as function of temperature were obtained for the pyrolysis of each fuel. A kinetic model was developed to interpret the similarities and differences regarding the fuel decomposition and species formation behaviors observed in the experiments. The fuel conversion of *n*-propylbenzene and *n*-butylbenzene proceeds along a similar curve, which is much faster than that of ethylbenzene. All three fuels are consumed mainly through the bond fission producing benzyl radical. The simultaneously formed C_1–C_3 alkyl radicals in separate cases significantly impact the fuel reactivity and the formation of small C_1–C_4 and monocyclic aromatic hydrocarbons. Specifically, in *n*-propylbenzene pyrolysis, the decomposition of ethyl radicals produces a considerable amount of hydrogen atoms, which enhances the reactivity of the reaction system and meanwhile results in relatively high production of benzene during the fuel consumption. The formation of other monocyclic aromatic hydrocarbon intermediates, such as toluene and styrene, is also influenced by fuel-related pathways. Concerning PAH formation, the kinetic schemes in the pyrolysis of linear C_8–C_{10} alkylbenzenes are very similar, which are dominated by the reactions of benzyl and other resonantly-stabilized radicals produced from benzyl decomposition. The major PAH formation reactions are barely influenced by the fuel chemistry. The only notable fuel-specific pathway is the indene formation from 1-phenyl-2-propenyl in *n*-propylbenzene and *n*-butylbenzene pyrolysis at relatively low temperatures. Styrene is an abundant product and its reaction with phenyl is found to be an important channel of phenanthrene formation.

1. Introduction

Alkylbenzenes are representative components of surrogates for practical fuels including gasoline [1], diesel [2] and kerosene [3]. C_8–C_{10} linear alkylbenzenes, namely, ethylbenzene, *n*-propylbenzene and *n*-butylbenzene are among the most frequently selected compounds when formulating a surrogate fuel. Apart from the necessity motivated by their wide application, their structural features make relevant combustion kinetic investigations appealing. C_8–C_{10} linear alkylbenzenes have an aromatic ring and a C_2–C_4 alkyl side chain in their molecules. Thus, their consumption potentially produces aromatic radicals such as benzyl and phenyl and C_1–C_4 alkyl radicals. Interactions among these radicals may greatly contribute to the formation and growth of polycyclic aromatic hydrocarbon (PAH) species under combustion conditions, and the reaction systems of C_8–C_{10} linear alkylbenzene fuels provide environments enabling investigations of such reactions.

The combustion kinetics of the individual aforementioned fuels was studied under various conditions through fundamental experiments and numerical approaches. Global combustion properties, such as ignition delay [4–6] and flame propagation and extinction [7–11], were measured using different facilities under broad

* Corresponding authors.
E-mail addresses: wenyu.sun@cnrs-orleans.fr (W. Sun), andrea.comandini@cnrs-orleans.fr (A. Comandini).

https://doi.org/10.1016/j.combustflame.2020.07.031

conditions. With regard to the chemical details, by monitoring the concentrations of fuels or the primary products, consumption pathways of C_8–C_{10} linear alkylbenzene were explored in early shock tube and static reactor pyrolysis studies [12–19]. Later, species concentration profiles in flow reactor pyrolysis [20–22] and laminar premixed flames [23–25] were obtained with the state-of-the-art photoionization molecular beam mass spectrometry technique at atmospheric or sub-atmospheric pressures. Species concentration profiles probed from jet-stirred reactor (JSR) oxidation experiments were also reported [20,21,26–29], mainly covering low-to-intermediate temperatures ($<$ 1200 K). In recent works [20–22,25], considerable attention was paid to developing predictive and widely-applicable kinetic models for each fuel, based on extensive validations against available datasets. Meanwhile, theoretical calculations were also performed [30,31] to refine the kinetic parameters of specific elementary reactions responsible for fuel consumptions. However, quantitative PAH speciation data in reaction systems of C_8–C_{10} linear alkylbenzenes at high-pressure conditions, which are highly concerned in practical operations, are rather sparse. To the best of our knowledge, the only relevant studies were reported by Gudiyella and Brezinsky [32,33] for *n*-propylbenzene oxidation and pyrolysis in a single-pulse shock tube at the pressure of 50 atm.

Sub-mechanisms for C_8–C_{10} linear alkylbenzenes are indispensable building blocks of kinetic models aimed at predicting the PAH speciation from the consumption of practical and surrogate fuels. Such kinetic models substantially benefit the numerical design of advanced clean combustion devices and the control over emissions from combustion processes. PAH formation kinetics in the pyrolysis of aromatic fuels was pursued in our recent works [34,35], based on the essential idea that a complicated combustion process can be potentially decouple to a pyrolysis and a subsequent oxidation steps [36]. A kinetic model was developed starting from the basic benzene and toluene [34], and then phenylacetylene, an intermediate on the Hydrogen-Abstraction-Acetylene-Addition (HACA) route resulting in the initial ring growth from benzene to naphthalene [35]. In the current work, the consumption and speciation kinetics of C_8–C_{10} linear alkylbenzenes is targeted. Pyrolysis experiments of highly argon-diluted fuel mixtures respectively containing 100 ppm of ethylbenzene, *n*-propylbenzene, and *n*-butylbenzene are performed in a single-pulse shock tube at a nominal pressure of 20 bar over a temperature range of 950–1700 K. Concentration profiles for species including small C_1–C_4 hydrocarbons, monocyclic aromatic species, and two- to four- ring PAH compounds are acquired through sampling and gas chromatography (GC) analysis. A kinetic model is developed by incorporating the sub-mechanisms of C_8–C_{10} linear alkylbenzenes and validated against the experimental results. Quantitative speciation measurements, joined by modeling analyses, are used to illustrate the common as well as fuel-specific pathways responsible for the similarities and differences among the three reaction systems. The influences of the lengths of the side chains in fuel molecules on the decomposition reactivity and the production of the PAH species are revealed.

2. Shock tube pyrolysis experiments

The pyrolysis experiments and the speciation analyses were performed on the single-pulse shock tube facility at ICARE, Orléans, France. Detailed descriptions of the single-pulse shock tube as well as the experimental procedures can be found in our previous works [34,35]. Briefly, the driven section of the shock tube is 78 mm in inner diameter and 3.7 m in length, and it is heated up to 90 °C to avoid condensation of heavy products. A dump tank, with a volume five times larger than the driven section, is connected to the driven section near the diaphragm for operation in single-pulse fashion. Four pressure sensors (CHIMIE METAL A25L05B) are mounted at an interval of 150 mm along the ending part of the driven section, with the last one being 82 mm away from the endwall. The recorded pressure signals are used to calculate the velocity of the incident shock wave, for the subsequent determination of the post-shock pressure and temperature conditions (p_5 and T_5) by solving the conservation equations based on ideal gas law and variable heat capacity ratio. A PCB pressure sensor shielded by a layer of room-temperature vulcanizing (RTV) silicone is placed on the endwall to record the pressure time history trace which is used to determine the reaction time for each experiment. Endwall pressure profiles at three different post-shock conditions are shown in Fig. S1 in the *Supplementary Material*. The definition of the reaction time is the duration from the arrival of the shock wave and the point when the pressure drops to 80% of p_5 due to the quenching effects of the rarefaction fan. The reaction time with the current experimental configuration is around 4.0 ms [34]. Other single-pulse shock tube facilities [37,38] traditionally depend on chemical thermometers for the determination of the post-shock conditions, T_5 and p_5, which are essentially averaged values throughout the reaction process [39]. Differently, in our experiments, we obtain T_5 and p_5 values at the beginning of the reaction time by solving the ideal shock wave relations, as mentioned above, and meanwhile provide a pressure history covering both the reaction time and the quenching period. Simulations with these parameters enable the consideration of the entire process experienced by the gas mixture in the shock tube. Therefore, the speciation of resonantly stabilized such as benzyl, which continue reacting during the quenching period, can be better described. Relevant details will be addressed in the discussion section. An air-operated HIP valve is connected to the endwall to sample the post-shock gas mixtures. The time of opening and closing of the valve is limited by mechanical constrains (hundreds of milliseconds), so a relatively large quantity of gas mixture (~20 ml at an equivalent pressure of about 1.5 bar) is sampled from the shock tube. The sampled mixtures are transferred through a SilcoTek tube heated at 210 °C to the GC system for subsequent analyses. The averaged shock wave velocity, instead of the extrapolated one at the endwall, is used to for the calculation of p_5 and T_5, so that the properties of the actual sampled gas can be better represented. The uncertainty in the calculated T_5 is estimated to be within $\pm$30 K, which mainly comes from the errors in the distances among the pressure sensors. The attenuation in the velocity was below 2.5% for most experiments, so the difference between the averaged or the extrapolated T_5 was below 20 K, within the uncertainty specified above. The gas sample is injected into the GC column when the pressure in the line is stabilized (usually taking a few seconds), and the injection pressure is recorded to normalize the GC signals for quantification. Two gas chromatography (GC) connected in series are responsible for the chemical composition analysis. The first GC (Agilent 7890) is equipped with a DB-17-ms column to separate heavy PAH compounds, and the signals are detected by a flame ionization detector (FID). The used injection pressure and the sample loop volume enable the sensitive detection of PAH species at sub-ppm level. A thermal conductivity detector (TCD) coupled to a Molsieve 5A column is mounted to monitor the absence of air and to evaluate the potential dilution effects of the helium gas from the driver section. An external valve box which can regulate the temperature up to 300 °C is used for this GC to minimize the loss of heavy compounds due to condensation. For the second GC (Thermo Trace GC Ultra), an FID connected to an HP Plot Q column is installed to measure the concentrations of small hydrocarbon products, and a DSQ mass spectrometer is connected to assist the species identification when necessary.

The calibrations of involved species were performed prior to the experiments, as detailed in [34]. Light hydrocarbons excluding diacetylene (C_4H_2), monocyclic aromatic hydrocarbon (MAH) species

and part of PAH species were calibrated using gas-phase standards with known compositions. C_4H_2 was calibrated from C_2H_2 pyrolysis experiments through the carbon atom conservation. For larger PAH species with low vapor pressures, the gas-phase calibration factors were obtained from liquid injections by taking acenaphthylene as a reference [34,35]. The uncertainty in the species concentration measurements mainly comes from the calibration processes: for species directly calibrated in gas phase, the uncertainty is expected to be within 5%–10%; for heavy compounds without direct calibrations, the measuring error can increase to 30%, depending on their molecular sizes relative to acenaphthylene. A good carbon balance (above 90%) is seen at relatively low temperatures (below 1300 K for ethylbenzene pyrolysis; below 1200 K for *n*-propylbenzene and *n*-butylbenzene pyrolysis). But the carbon recoveries, contributed by identified species, deteriorate in high-temperature regimes, down to around 75%. This is mainly because larger polyacetylenes such as C_6H_2 and C_8H_2 are not identified in our experiments. Particularly, relatively large amounts of C_6H_2 are expected to be produced at high temperatures from the decomposition of aromatic rings and the subsequent reactions among C_2H_2, C_2H, C_4H_2 and C_4H. Besides, heavy PAHs larger than four-ring species cannot be measured with the current experimental facility, and soot particles may also be formed under the high-pressure, pyrolytic conditions with aromatic fuels. All the experimental measurements, including the reaction time, the post-shock conditions (T_5 and p_5) and the species concentrations, are provided in the *Supplementary Material*.

The experiments were performed at a nominal p_5 of 20 bar, with T_5 ranging from 950 K to 1700 K. Three highly argon-diluted mixtures, respectively containing 101 ppm ethylbenzene, 103 ppm *n*-propylbenzene and 102 ppm *n*-butylbenzene, were prepared in a 136 L electropolished stainless steel cylinder and kept for overnight to homogenize before experiments. The chemicals (ethylbenzene, 99.8%; *n*-propylbenzene, >99%; *n*-butylbenzene, >99%) were purchased from Sigma-Aldrich and the argon (>99.9999%) gas was supplied by Air Liquide. The driven section of the shock tube was vacuumed to below 10^{-5} torr with a molecular turbo pump before introducing the experimental gas mixture in each operation. To point out, the initial fuel concentration was chosen to be 100 ppm in the current experiments, which was halved in comparison to that used previously for toluene pyrolysis experiments [34], to avoid clogging of the analytical system caused by soot particles formed during pyrolysis and sampled into the GC lines. Besides, the inner surface of the driven section was cleaned every day to remove carbon deposits.

3. Kinetic modeling

The kinetic model developed in this work is aimed at correctly reproducing the decomposition of C_8–C_{10} linear alkylbenzene fuels and the formation of PAH species under shock tube pyrolysis conditions. Such efforts are made as a continuation of our serial works [34,35] towards constructing a predictive kinetic model describing PAH speciation behaviors of aromatic practical and surrogate fuels under combustion related conditions. The kinetic model for C_8–C_{10} linear alkylbenzenes pyrolysis has a typical hierarchical structure, given the fact that relevant radicals or intermediates of a smaller alkylbenzene decomposition can also be formed from the consumption of larger ones. During the pyrolysis of C_8–C_{10} alkylbenzenes, toluene, the simplest alkylbenzene, is an important intermediate and relevant pathways starting from benzyl (C_7H_7) can be crucial sources of PAH formation. A sub-mechanism of the PAH speciation from toluene decomposition was developed and validated in our recent work [34]. It laid the foundation for the kinetic model for alkylbenzenes pyrolysis by serving as an essential secondary sub-mechanism. For important reactions incorporated in the current kinetic model, specifically, the C_8–C_{10} alkylbenzenes consumption steps and some fuel-specific PAH formation pathways, the adopted rate coefficients are listed in Table S1 in the *Supplementary Material*.

A detailed sub-mechanism for ethylbenzene consumption was already included in earlier versions of our kinetic model [34,35]. The unimolecular decomposition reactions are expressed in reverse form by using the theoretical rate coefficients reported by Matsugi and Miyoshi [40]. Rate constants for ipso substitution reactions and hydrogen abstraction reactions by H, CH_3 and C_6H_5 are taken from the ethylbenzene kinetic model proposed by Yuan et al. [20]. The consumption reactions of the two fuel radicals 1-phenylethyl ($C_6H_5\dot{C}HCH_3$) and 2-phenylethyl ($C_6H_5CH_2\dot{C}H_2$) and corresponding rate constants are from the theoretical work by Tokmakov and Lin [41]. In our previous model [34,35], the *n*-propylbenzene sub-mechanism, which originates from the CRECK model [42], is highly-lumped, and the *n*-butylbenzene sub-mechanism is absent. Therefore, these two sub-mechanisms are updated or supplemented in the current work. Rate coefficients for the unimolecular decomposition reactions of both *n*-propylbenzene and *n*-butylbenzene are from the kinetic model by Diévart and Dagaut [27]. For hydrogen abstractions by H and CH_3, the theoretically determined rate coefficients reported by Robinson and Lindstedt [30] are adopted for reactions of *n*-propylbenzene directly, and for the reactions of *n*-butylbenzene via analogies. Rate coefficients for hydrogen abstractions by other radicals, including C_2H_5, C_6H_5 and C_7H_7 are from the work by Diévart and Dagaut [27]. The consumption reactions of *n*-propylbenzene fuel radicals as well as corresponding rate coefficients are taken from a recent kinetic model proposed by Jin et al. [43], while for the consumption scheme of *n*-butylbenzene fuel radicals, rate coefficients from the work by Zhang et al. [22] are adopted. For fuel radical decomposition rate coefficients from [20,22], their pressure-dependence is kept in the current kinetic model, though high-pressure limits should be enough to characterize relevant kinetics at the pressure of 20 bar. This may benefit the future model development to predict measurements acquired at different pressures.

Regarding the PAH formation pathways, reaction sequences starting from benzyl leading to two-to four- ring PAH species were addressed in our previous work [34]. In this work, attention is paid to specific pathways more relevant to the fuel structures. Potential direct formation of PAH species containing the same carbon atoms as the fuels, namely the formation pathways of indene (C_9H_8) from *n*-propylbenzene and naphthalene ($C_{10}H_8$) from *n*-butylbenzene pathways are considered in the model construction, as shown in Scheme 1. C_9H_8 and dihydro-naphthalene ($C_{10}H_{10}$) are produced through ring closure steps of 1-phenyl-2-propenyl ($CC_6H_5C_3H_4$–1) and phenyl-butenyl radicals ($AC_6H_5C_4H_6$–2 and $AC_6H_5C_4H_6$–3), respectively. The consumption of $C_{10}H_{10}$ can further result in $C_{10}H_8$ formation via losing either two hydrogen atoms or a hydrogen molecule. Besides, 1,3-butadienyl-benzene ($C_6H_5C_4H_5$) can lead to the formation of 1-methyleneindanyl radical ($C_9H_7CH_2$) which further transforms into $C_{10}H_8$ through ring-rearrangement. Rate coefficients for the involved reactions are taken from recent kinetic models [21,22]. Styrene ($C_6H_5C_2H_3$) is produced in large concentrations in the pyrolysis experiments of the three investigated fuels. Inspired by the finding that phenanthrene can be largely produced from the phenylacetylene and phenyl addition-elimination reactions, as discussed in our recent work [35], analogous reaction sequences between styrene and phenyl producing 9,10-dihydro-phenanthrene ($C_{14}H_{12}$) are considered in the model construction, and the decomposition of $C_{14}H_{12}$ further yields phenanthrene ($C_{14}H_{10}$) through dehydrogenation processes, similar to the above-mentioned $C_{10}H_8$ formation from $C_{10}H_{10}$ consumption.

Consistent with our previous works [34,35], all simulations in the present work were performed with the homogenous reactor

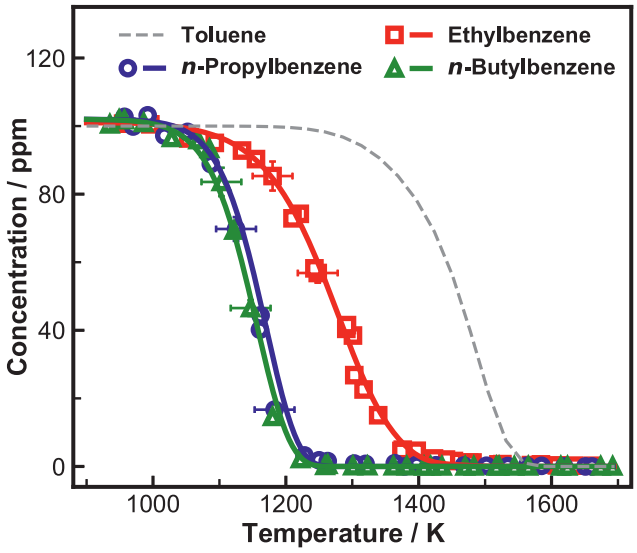

Fig. 1. Experimental (symbols) and simulated (solid lines) fuel concentrations as a function of T_5 in C_8–C_{10} linear alkylbenzenes pyrolysis. Simulated fuel conversion profile in 100 ppm toluene pyrolysis is shown as the dashed line for comparison purpose.

model of the software COSILAB [44] with a nominal reaction time of 4.0 ms and a constant pressure of 20 bar. The constant pressure assumption typically used in simulating the speciation results sampled from single-pulse shock tube experiments have been well justified in previous publications [39,45].

4. Results and discussion

In this section, experimental and simulated species concentrations as a function of temperature will be shown in conjunction to verify the predictive abilities of the kinetic model. More importantly, by combining high-fidelity measurements and analyses with a predictive kinetic model, the different decomposition reactivity and speciation of the three investigated alkylbenzenes as well as the responsible reaction schemes are revealed in a comparative way. To facilitate a more comprehensive comparison, the case of toluene pyrolysis at the initial concentration of 100 ppm will be shown as a reference through modeling approach when needed.

4.1. Fuel decomposition and small hydrocarbon products

The fuel conversion curves as a function of the temperature for C_8–C_{10} alkylbenzenes under nearly identical conditions (initial concentration of 100 ppm, nominal pressure of 20 bar and reaction time of 4.0 ms) are displayed in Fig. 1. The fuel decomposition reactivity can be accurately captured by the kinetic model. The fuel decay of C_8–C_{10} alkylbenzenes occur at significantly lower temperatures, compared to their simpler counterpart toluene. The decomposition of *n*-propylbenzene and *n*-butylbenzene have a similar pattern, while proceeding at a faster pace and covering a lower temperature window, compared to ethylbenzene decomposition. It has been well-established that the thermal decomposition of alkylbenzenes are dominated by bond fissions producing benzyl (C_7H_7). The strengths of the C–C bonds adjoining the benzyl moiety in the three molecules can partly explain the order of their decomposition reactivity. For such benzylic C–C bonds, the bond dissociation energies (BDEs) in *n*-propylbenzene and *n*-butylbenzene have close values ($C_6H_5CH_2$–C_2H_5, 75.3 kcal/mol; $C_6H_5CH_2$–C_3H_7, 74.9 kcal/mol [46]), slightly lower than that in ethylbenzene ($C_6H_5CH_2$–CH_3, 76.4 kcal/mol [46]). Besides, the longer side chains in *n*-propylbenzene and *n*-butylbenzne provide more possibilities for bond fissions and radical attacks. As for the almost identical decomposition reactivity of *n*-propylbenzene and *n*-butylbenzene, explanations will be given in the following discussion.

Experimental and simulated concentration profiles of C_1–C_4 hydrocarbons during the pyrolysis of ethylbenzene, *n*-propylbenzene and *n*-butylbenzene are shown in Figs. 2, 3 and 4, respectively. The small hydrocarbons are quantitively different in the pyrolysis of C_8–C_{10} linear alkylbenzenes, some of them already start to form at the initial stage of the fuel consumption. The model can satisfactorily reproduce the measurements in separate cases and more importantly, it can well capture the differences among the three cases. To interpret potential correlations between the speciation and fuel structural features in alkylbenzenes pyrolysis, initial fuel consumption pathways based on the rate-of-production (ROP) analyses in the three reaction systems are presented in Figs. 5, 6 and 7. The temperatures chosen to perform the ROP analyses are 1250 K for ethylbenzene pyrolysis, and 1150 K for *n*-propylbenzene and *n*-butylbenzene pyrolysis, at which nearly half of the fuel is consumed in each case.

It is noted that both methane (CH_4) and ethane (C_2H_6) have similar peak concentrations in the pyrolysis of ethylbenzene and *n*-butylbenzene, and obviously higher than those in the case of *n*-propylbenzene, though the speciation of *n*-propylbenzene and *n*-butylbenzene are expected to share more similarities. The formation of both CH_4 and C_2H_6 are closely related to the consumption reactions of methyl radical (CH_3). The simulated concentration profiles of CH_3 in the pyrolysis of the three alkylbenzene fuels are provided in Fig. S2 in the *Supplementary Material*. CH_3 concentrations are the lowest in *n*-propylbenzene pyrolysis, which can be explained by the initial fuel consumption steps. As mentioned above, the bond fissions leading to C_7H_7 dominate the consumption of individual fuels, and such reactions meanwhile lead to the formation of CH_3, ethyl (C_2H_5) and *n*-propyl (n-C_3H_7) in the cases of ethylbenzene, *n*-propylbenzene and *n*-butylbenzene, respectively. The consumption of n-C_3H_7 is mainly through the C–C β-scission (n-$C_3H_7 \rightarrow CH_3+C_2H_4$) resulting in a high production of CH_3. The consumption of C_2H_5 is dominated by the reaction $C_2H_5 \rightarrow C_2H_4+H$, while the channel leading to CH_3 formation ($C_2H_5+H = 2CH_3$) only has a moderate contribution. CH_3 radicals can undergo self-combination or combine with other radicals including H, C_6H_5 and C_7H_7, and these chain-termination reactions account for the lower-than-expected reactivity of *n*-butylbenzene: even a longer side chain exists in its molecule, it has similar decomposition reactivity with *n*-propylbenzene (see Fig. 1). During the decomposition of ethylbenzene, ethylene (C_2H_4) can be produced from the decomposition of the fuel radical $C_6H_5C_2H_4$ and C_2H_5. Both $C_6H_5C_2H_4$ and C_2H_5 can be formed through specific fuel decomposition pathways, whose importance is however quite minor compared to the dominant C_7H_7 producing channel, which accounts for 79% of the fuel decomposition under the conditions concerned in Fig. 5. In the pyrolysis of *n*-propylbenzene and *n*-butylbenzene, C_2H_4 can be largely produced from the decomposition of the above-mentioned important radicals C_2H_5 and n-C_3H_7 through $C_2H_5 \rightarrow C_2H_4+H$ and n-$C_3H_7 \rightarrow CH_3+C_2H_4$, respectively. Similar explanation can be applied to the distinct propylene (C_3H_6) concentrations observed in the three reaction systems: In the pyrolysis of ethylbenzene, no fuel-related pathway leads to the formation of C_3H_6 which is mainly produced from un inefficient addition-elimination channel $C_2H_4+CH_3 \rightarrow C_3H_6+H$; and during *n*-propylbenzene pyrolysis, C_3H_6 mainly comes from the consumption of the fuel radical $C_6H_5CH_2\dot{C}HCH_3$ which however takes limited carbon flux (see Fig. 6). Differently, in the pyrolysis of *n*-butylbenzene, C_3H_6 can be formed from the decomposition of the fuel radical $C_6H_5CH_2CH_2\dot{C}HCH_3$ as well as the abun-

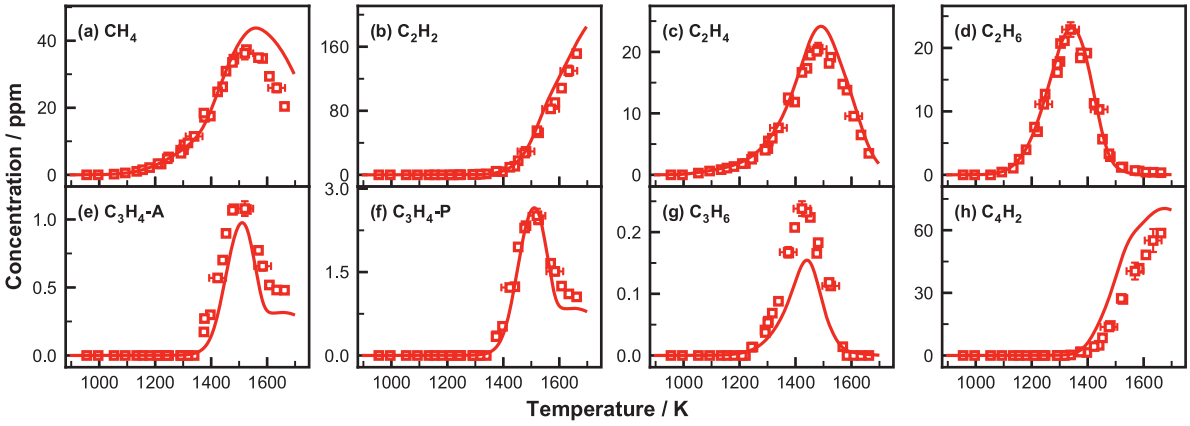

Fig. 2. Experimental (symbols) and simulated (lines) concentrations of small hydrocarbon products as a function of T_5 in ethylbenzene pyrolysis.

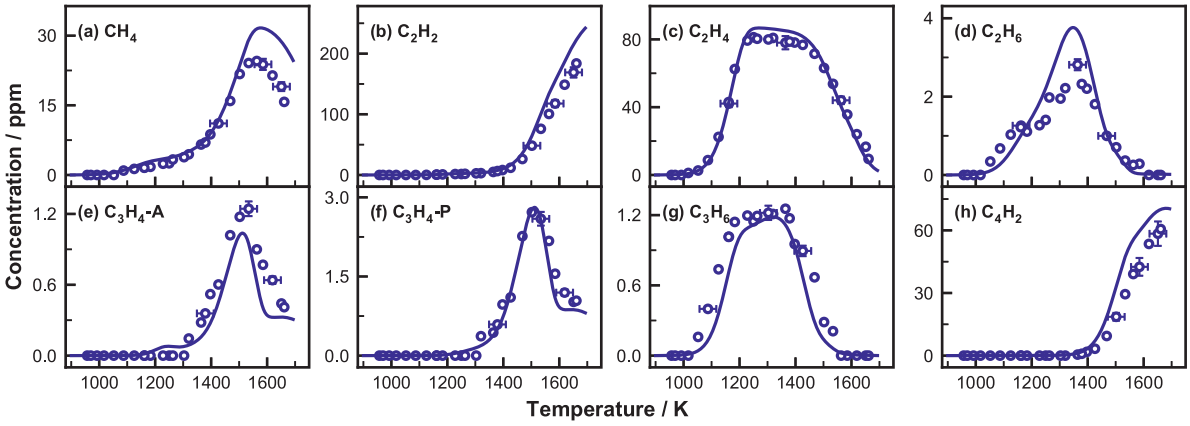

Fig. 3. Experimental (symbols) and simulated (lines) concentrations of small hydrocarbon products as a function of T_5 in *n*-propylbenzene pyrolysis.

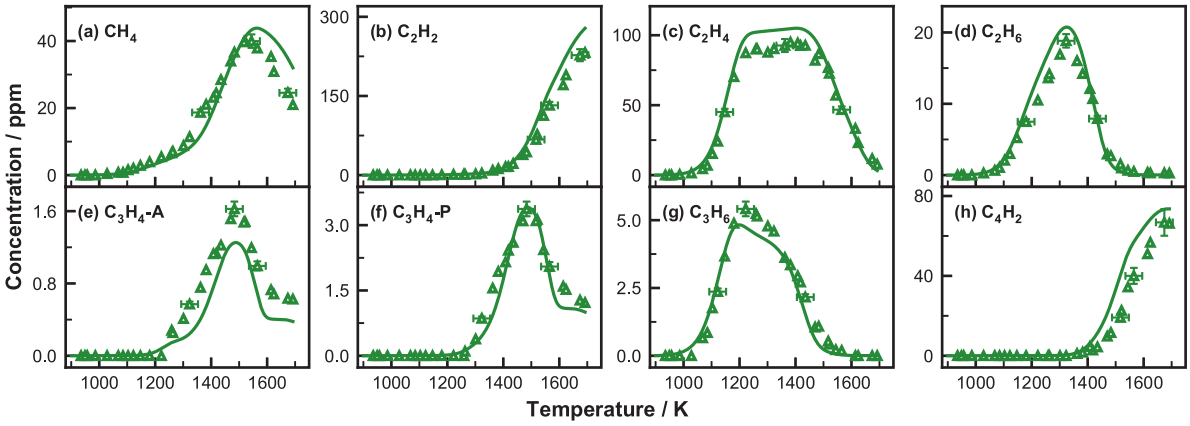

Fig. 4. Experimental (symbols) and simulated (lines) concentrations of small hydrocarbon products as a function of T_5 in *n*-butylbenzene pyrolysis.

dant *n*-C_3H_7 (see Fig. 7). In all the three cases, the C_3H_4 isomers, propyne (C_3H_4-P) and allene (C_3H_4-A) are produced at relatively high temperatures where the fuels are depleted. The consumption of C_3H_6 leads to the formation of C_3H_4-A which further isomerizes to C_3H_4-P. The concentrations of C_3H_4-A and C_3H_4-P both increase with the increasing length of the side chain in the fuel molecules. It is noteworthy that the C_3H_4 isomers peak at the same temperature and the ratio of their peak concentrations (C_3H_4-A/C_3H_4-P) remain at 45% in all three cases, indicating a stable balance between the two isomers regardless of the fuels. Similar observation for the C_3H_4 isomers was also reported by Hansen et al. [47] through a data research involving 55 sets of premixed flame chemical structure measurements. For the dominant high-temperature pyrolysis products acetylene (C_2H_2) and diacetylene (C_4H_2), their concentrations increase with the fuel molecular sizes, as they are closely related to the carbon contents in the reaction systems.

To better understand and compare the processes that control the consumption of C_8–C_{10} linear alkylbenzenes, sensitivity analy-

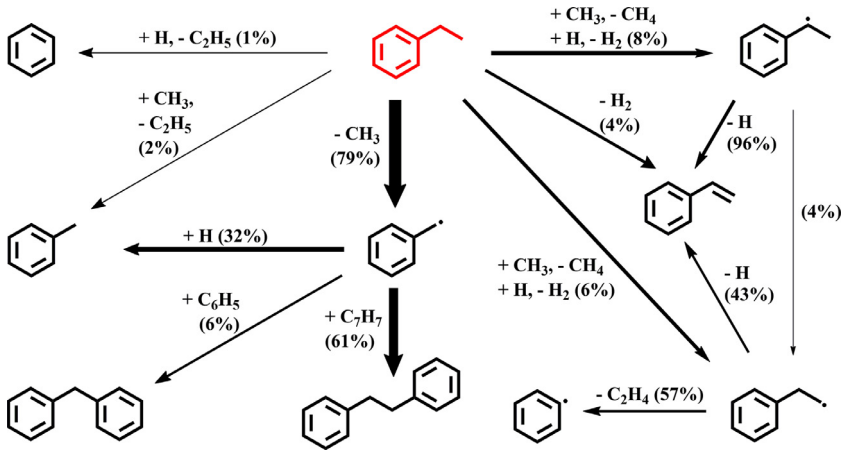

Fig. 5. Fuel consumption pathways in ethylbenzene pyrolysis at 1250 K. The thickness of the arrows represents the carbon flux through the corresponding reactions, and the percentage numbers are the contributions by corresponding reactions to the consumption of the species on the source side.

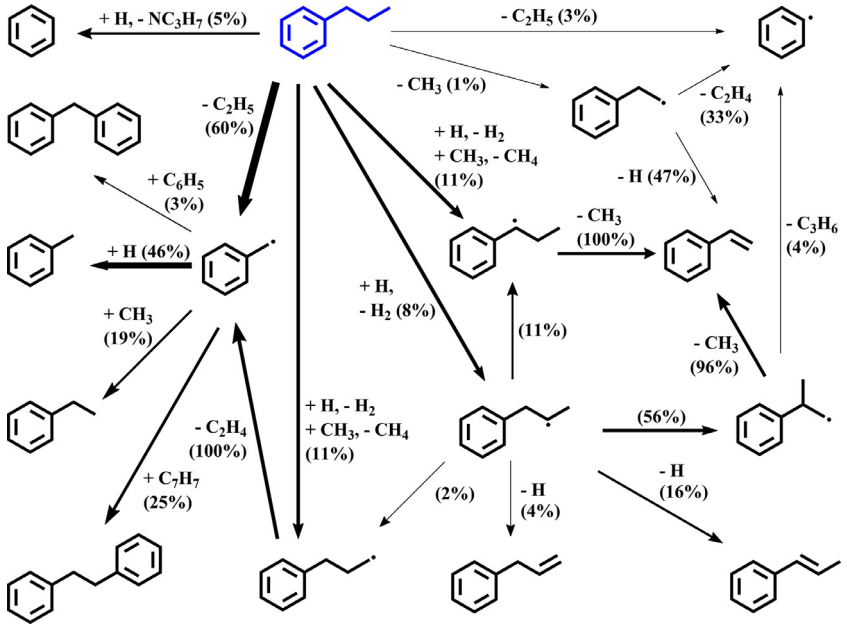

Fig. 6. Fuel consumption pathways in *n*-propylbenzene pyrolysis at 1150 K. The thickness of the arrows represents the carbon flux through the corresponding reactions, and the percentage numbers are the contributions by corresponding reactions to the consumption of the species on the source side.

ses for fuel concentrations are performed at temperatures where the fuel conversion ratios are around 50% (T_5 = 1250 for ethylbenzene, T_5 = 1150 for *n*-propylbenzene and *n*-butylbenzene), and the results are shown in Fig. 8. For all the three fuels, the benzylic C–C bond fissions have the highest sensitivity coefficients facilitating fuel consumption, which is consistent with their dominance in the reaction flux discussed above. Another similarity shared in the sensitivity spectra of the three fuels is that the reaction $C_7H_8(+M) = H + C_7H_7(+M)$ inhibits the fuel consumption. In the reaction systems of C_8–C_{10} linear alkylbenzene pyrolysis, this reaction proceeds in the backward direction, resulting in toluene (C_7H_8) formation and consuming the important chain carriers H atoms. It is noteworthy that the chain terminating CH_3 self-combination promotes the ethylbenzene decomposition. The probable reason is that this reaction effectively removes CH_3 from the reaction system, which can otherwise recombine with the stabilized C_7H_7 to form ethylbenzene molecules. Hydrogen abstraction reactions by CH_3, which consume both the fuel and CH_3, facilitate the consumption of ethylbenzene. CH_3 related reactions have minor influences on fuel consumption in *n*-propylbenzene and *n*-butylbenzene pyrolysis, where hydrogen abstraction reactions by H are relatively more important due to the higher contents of H atoms.

4.2. The formation of MAH species

Since an aromatic ring already exists in the fuel molecule, monocyclic aromatic hydrocarbon (MAH) species are produced in large quantities from the pyrolysis of C_8–C_{10} linear alkylbenzenes. The experimental and modeling concentrations of MAH species are shown in Fig. 9 as a function of the temperature. The simulated species concentration profiles in 100 ppm toluene pyrolysis are also shown as a reference. Benzene (C_6H_6) is abundant in the pyrolysis of all three fuels, and regarding its speciation patterns in the three cases, those in ethylbenzene and *n*-butylbenzene pyrolysis share more similarities while that in *n*-propylbenzene pyrolysis exhibits different behaviors. A two-stage formation can be seen in the profiles of C_6H_6 in each case, including a slow production in relatively low temperature ranges around 1100–1350 K and a rapid increase at higher temperatures till around 1500 K. The C_6H_6

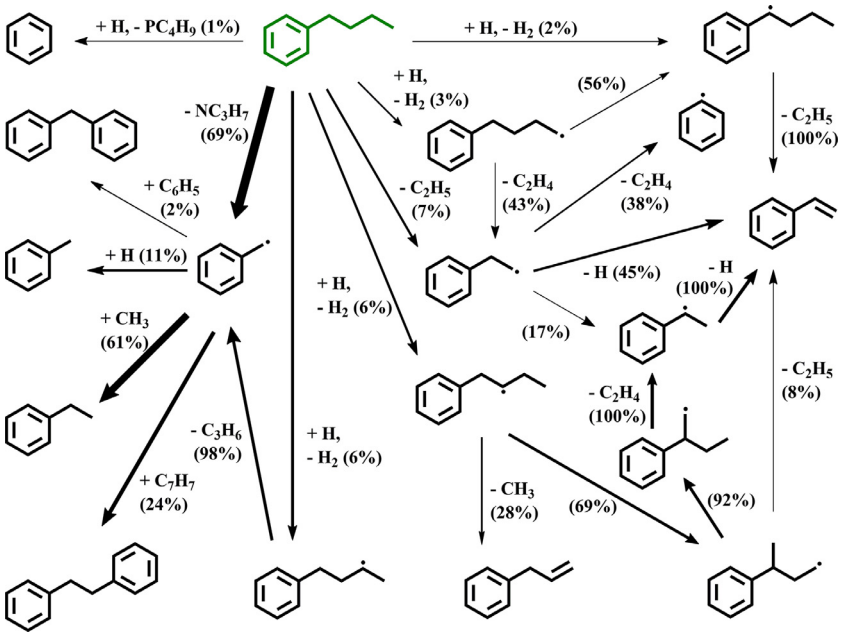

Fig. 7. Fuel consumption pathways in *n*-butylbenzene pyrolysis at 1150 K. The thickness of the arrows represents the carbon flux through the corresponding reactions, and the percentage numbers are the contributions by corresponding reactions to the consumption of the species on the source side.

concentration profile in *n*-propylbenzene pyrolysis exhibits unique characteristics in the first stage of formation: a remarkably higher production and a platform from 1200 to 1300 K. For the second stage of C_6H_6 formation, the concentration profiles in the pyrolysis of C_8–C_{10} alkylbenzenes are more similar, and they resemble that in toluene pyrolysis. Over the entire temperature range, the C_6H_6 concentrations are the highest in the pyrolysis of *n*-propylbenzene, followed by *n*-butylbenzene, and ethylbenzene, and such trend can be faithfully captured by the kinetic model predictions.

To understand the kinetics responsible for the different C_6H_6 formation behaviors among the three cases, time-resolved ROP-analyzed results for C_6H_6 at 1250 K and 1500 K, which are representative of the two formation stages, are shown in Fig. 10. The time axis is presented in logarithmic scale for the ROP results at 1500 K, because specific reactions have intense contributions in narrow time ranges under high-temperature conditions. The formation of C_6H_6 is dominated by the ipso substitution reactions between the fuel and H atom at 1250 K in each case. Figure S2(b) shows that a higher level of H atoms presents in the pyrolysis of *n*-propylbenzene than other fuels, because the consumption of *n*-propylbenzene results in plentiful C_2H_5 radicals which subsequently decompose and release H atoms through the reaction $C_2H_5(+M) = C_2H_4+H(+M)$. The reaction $C_6H_5+H(+M) = C_6H_6(+M)$ also contributes to C_6H_6 formation, and its importance is in accordance with the levels of H atoms in the three reaction systems. In *n*-propylbenzene and *n*-butylbenzene pyrolysis, the ipso substitution reactions of smaller alkylbenzenes with H atoms, *i.e.* $H + C_7H_8 = C_6H_6+CH_3$ and $H + C_6H_5C_2H_5 = C_6H_6+C_2H_5$, are other sources of C_6H_6, and the relative importance of these two reactions is correlated to the concentrations of C_7H_8 and $C_6H_5C_2H_5$ (see Fig. 9(b) and (e)). The recombination reactions, $C_7H_7+H \rightarrow C_7H_8$ and $C_7H_7+CH_3 \rightarrow C_6H_5C_2H_5$, prevail the formation of C_7H_8 and $C_6H_5C_2H_5$, respectively. The higher H production in *n*-propylbenzene pyrolysis and the higher CH_3 production in *n*-butylbenzene pyrolysis results in the different concentrations of C_7H_8 and $C_6H_5C_2H_5$ observed in the experiments. This point is also revealed by the different fates of C_7H_7 along the consumption pathways of *n*-propylbenzene and *n*-butylbenzene, as can be noted from Figs. 6 and 7. Figure 10(b) indicates that at higher temperatures, the ipso substitution reactions of the fuels are no longer important contributors to C_6H_6 formation. The reaction $C_6H_5+H(+M) = C_6H_6(+M)$ still plays an important role in C_6H_6 formation in the pyrolysis of all three fuels, especially in *n*-propylbenzene and *n*-butylbenzene pyrolysis, where H atoms have higher concentrations, and it has remarkable effects in a very short period (with the magnitude of microseconds) at the beginning. The contributions from the reactions of small molecules, such as the recombination of propargyl (C_3H_3), are delayed by about 10^{-1} ms, but covering a much wider time scale. The decomposition of styrene ($C_6H_5C_2H_3$), $C_6H_5C_2H_3 = C_6H_6+H_2CC$, plays an important role over almost the entire reaction time in all three cases.

$C_6H_5C_2H_3$ is among the initial products of C_8–C_{10} linear alkylbenzenes pyrolysis, as its formation starts at relatively lower temperatures than other MAH species. It has similar peak concentrations in C_8–C_{10} linear alkylbenzenes pyrolysis, whereas much higher than that in toluene pyrolysis. However, the concentrations evolve with the temperature in distinct manners in the three cases. In ethylbenzene pyrolysis, a relatively late peak shows in the $C_6H_5C_2H_3$ concentration profile which is composed of a continuous increase and decrease. The $C_6H_5C_2H_3$ concentration profile in *n*-propylbenzene pyrolysis exhibit a fast rise ahead of a two-stage decrease, and the first decrease over 1200–1400 K is moderate, resulting in a small shoulder after the peak. For that in *n*-butylbenzene, the increasing phase contains a rapid increase followed by a mild one, yielding a peak concentration at about 1350 K. The kinetic model is able to capture the trend in each case despite an overestimation in *n*-butylbenzene pyrolysis. The $C_6H_5C_2H_3$ formation from ethylbenzene pyrolysis is mainly through the decomposition of phenylethyl radicals ($C_6H_5\dot{C}HCH_3$ and $C_6H_5CH_2\dot{C}H_2$) throughout the temperature window. At relatively low temperatures, the rapid $C_6H_5C_2H_3$ formation in both *n*-propylbenzene and *n*-butylbenzene pyrolysis arises from the decomposition of fuel radicals $C_6H_5\dot{C}HCH_2CH_3$ ($C_6H_5C_3H_6$–C) and $C_6H_5\dot{C}HCH_2CH_2CH_3$ ($C_6H_5C_4H_8$-D), respectively, as shown in Figs. 6 and 7. Remarkably different behaviors exist in the second stages of their speciation profiles where the fuel is just depleted and the $C_6H_5C_2H_3$ formation is taken over by phenylethyl

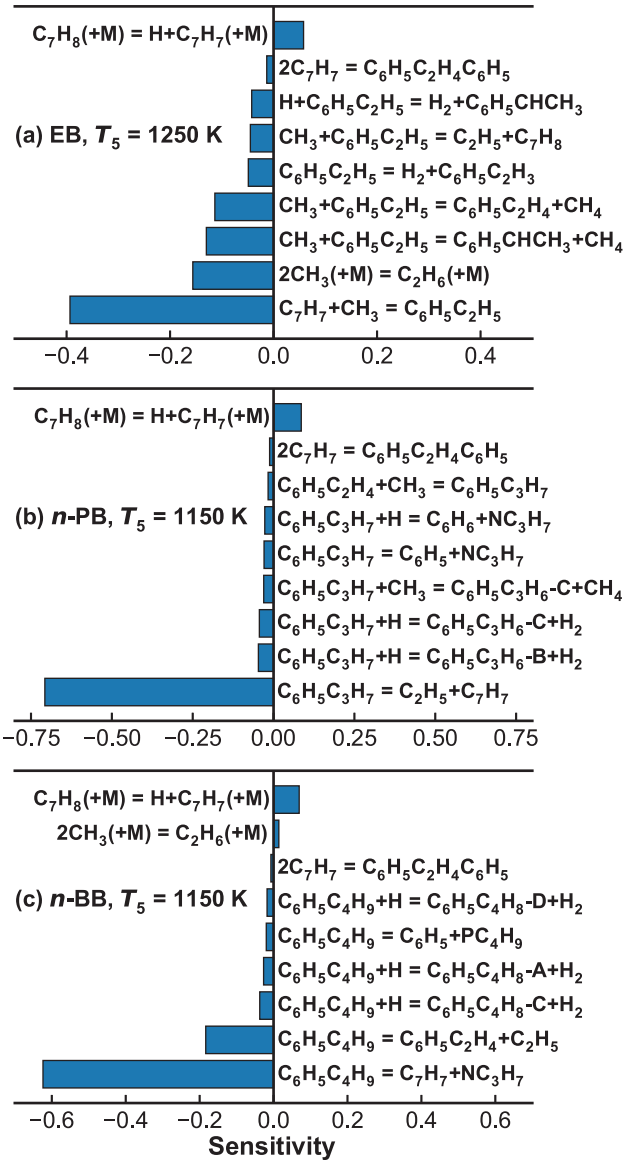

Fig. 8. Sensitivity analysis for fuel concentration at temperatures where about half of the fuel is consumed in each case of C_8–C_{10} linear alkylbenzenes pyrolysis.

radicals decomposition. The higher production of phenylethyl radicals in *n*-butylbenzene gives rise to more obvious compensating effects over the fuel depletion and thus a second concentration increase. On the other hand, for phenylacetylene ($C_6H_5C_2H$) which also has a molecular structure containing an aromatic ring and a C_2 side chain, the peak concentrations are similar among the pyrolysis of all alkylbenzenes ranging from toluene to *n*-butylbenzene, as shown in Fig. 9(d). The formation of $C_6H_5C_2H$ starts at relatively high temperatures and barely influenced by the fuel chemistry. It is dominated by the ethynyl radical (C_2H) addition to phenyl (C_6H_5). The consumption of styryl radicals ($C_6H_5\dot{C}CH_2$ and $C_6H_5C\dot{H}CH$) also have certain contributions at relatively low temperatures, which explains the lower formation temperatures in C_8–C_{10} alkylbenzenes pyrolysis compared to that toluene pyrolysis. The decomposition phases of $C_6H_5C_2H$ speciation curves in all shown cases including toluene pyrolysis coincide, which is mainly through the addition-elimination reaction $C_6H_5C_2H+H = C_6H_5+C_2H_2$.

4.3. The formation of PAH species

Measured and simulated concentrations of two- to four-ring PAH species produced from C_8–C_{10} linear alkylbenzenes pyrolysis over the temperature range of 950–1700 K are displayed in Fig. 11. Overall, the kinetic model can well predict the experimental results, regarding the shapes and sizes of individual speciation profiles, except for an obvious under-prediction in bibenzyl ($C_6H_5C_2H_4C_6H_5$) concentrations, which will be explained later in this section. The PAH species concentration distributions are roughly comparable among the pyrolysis of ethylbenzene, *n*-propylbenzene and *n*-butylbenzene, though some differences in specific species profiles are noticeable. These similarities and differences can be satisfactorily captured by the model predictions. Based on the valid predictive ability of the kinetic model, a major goal of the current study is to compare the PAH formation pathways in the pyrolysis of C_8–C_{10} alkylbenzenes, and to reveal the influences brought by the fuel structural features, namely the different lengths of the side chains. The case of 100 ppm toluene pyrolysis is also simulated, and the modeling profiles for PAH species are shown as a reference in Fig. 11 to benefit more comprehensive comparisons.

Figure 11 suggests that whether a PAH species has different speciation behaviors in C_8–C_{10} alkylbenzenes pyrolysis largely depends on its temperature window. The formation of biphenylmethane ($C_6H_5CH_2C_6H_5$) and bibenzyl ($C_6H_5C_2H_4C_6H_5$) (see Fig. 11(d) and (e)) starts at relatively low temperatures through $C_7H_7+C_6H_5$ recombination and C_7H_7 self-recombination, respectively. Their temperature windows overlap with those of the fuel decomposition in each case. They are the two PAH species whose speciation behaviors are influenced the most by the fuel structures, because their formation requires the participation of only C_7H_7 and C_6H_5 which are among the dominant primary products of alkylbenzenes decomposition. According to the measurements, $C_6H_5C_2H_4C_6H_5$ is the most abundant PAH species in the pyrolysis of C_8–C_{10} alkylbenzenes. However, the model obviously "under-predicts" $C_6H_5C_2H_4C_6H_5$ concentrations though it still captures the relative trends among the three experimental sets. It is pointed out by Martens et al. [48] that reactions involving specific stabilized radicals can carry on during the quenching period. Due to the resonance stability of C_7H_7, the modeling $C_6H_5C_2H_4C_6H_5$ concentrations shown in Fig. 11(e), which are based on the assumption that reactions are instantaneously quenched by the arrival of rarefaction waves, could be remarkably impacted. Simulations with measured pressure profiles are carried out to examine this issue. Figure 12 displays time-dependent concentrations of C_7H_7 radical and PAH species in individual shocks at around 1400 K from respective experimental sets. Large amounts (up to 10 ppm) of C_7H_7 survive the shock heating and continue to react during the quenching period. Bibenzyl exhibits a unique speciation behavior: it is formed rapidly in a very short time range at the beginning of the reaction time; then it is gradually consumed by participating in the formation of other species, and afterwards, produced again till reaching its final concentrations during the quenching period. At T_5 = 1400 K, simulated $C_6H_5C_2H_4C_6H_5$ concentrations at 4.0 ms are below 50% of the final values, which are more representative of the experimental measurements. Differently, the formation of other PAH species is essentially completed before the post-shock cooling, as indicated by the plateaus in their concentrations.

Simulations were performed with measured pressure profiles, up to a time scale of 10 ms to obtain the final species concentrations which do not evolve with the time anymore. The resulting $C_6H_5C_2H_4C_6H_5$ concentrations as a function of T_5 are presented in Fig. 13, together with the corresponding measurements and modeling results at a constant pressure of 20 bar within a fixed reaction

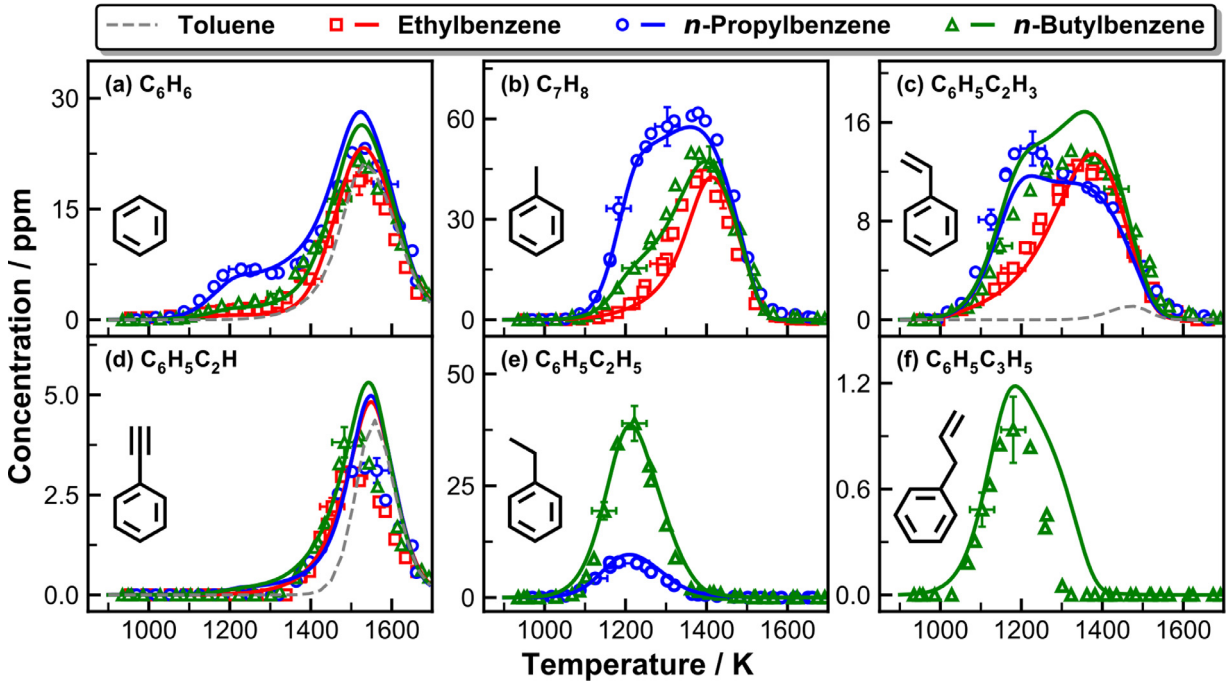

Fig. 9. Experimental (symbols) and simulated (lines) concentrations of MAH products as a function of T_5 in C_8–C_{10} linear alkylbenzenes pyrolysis. Simulated speciation profile in 100 ppm toluene pyrolysis are shown as the dashed lines for comparison purpose.

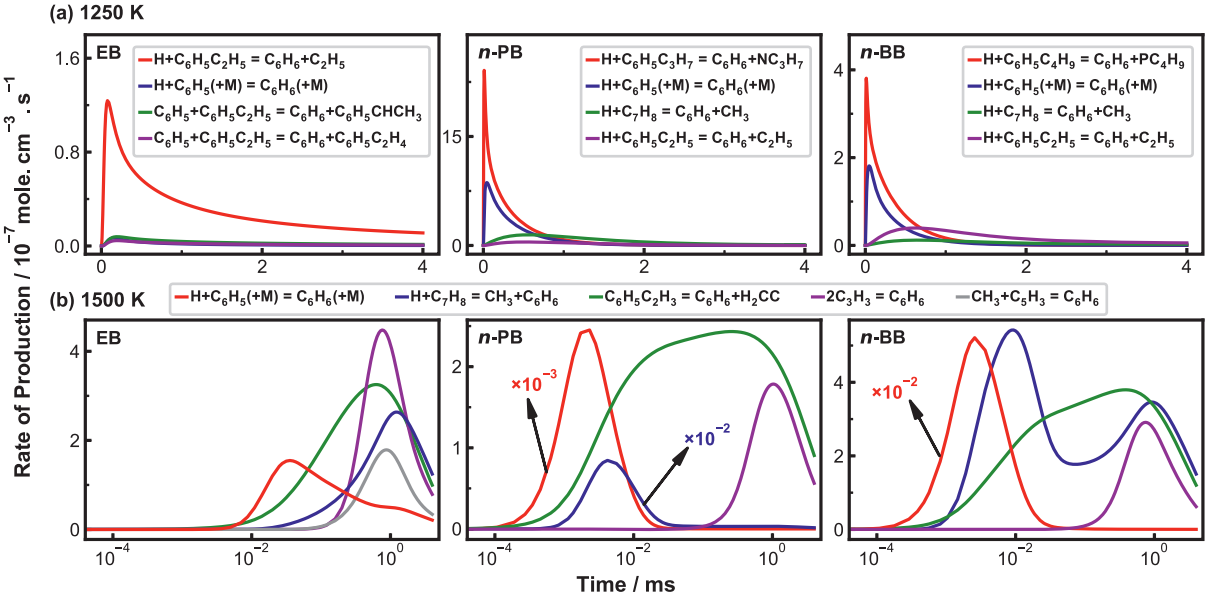

Fig. 10. Rate of production analysis for C_6H_6 over the reaction time of 4.0 ms in C_8–C_{10} linear alkylbenzenes pyrolysis at (a) 1250 K and (b) 1500 K. The time is displayed in logarithmic coordinates in the cases at 1500 K.

time of 4.0 ms. Those for other species in the pyrolysis of ethylbenzene, *n*-propylbenzene and *n*-butylbenzene are provided in Figs. S3, S4 and S5, respectively, in the *Supplementary Material*. The simulations with pressure profiles can better match the measurements for $C_6H_5C_2H_4C_6H_5$ in all three cases. For other species, the simulation methods do not obviously alter the modeling concentration profiles, except for slight increases in indene (C_9H_8) concentrations at relatively high temperatures above 1400 K. This mainly lies in a moderate continuation of the reaction $C_7H_7+C_2H_2 = C_9H_8+H$ during the cooling period.

The production of $C_6H_5C_2H_4C_6H_5$ in C_8–C_{10} alkylbenzene pyrolysis is much higher than that in toluene pyrolysis. This is because the decomposition of C_8–C_{10} alkylbenzenes starts at relatively low temperatures (below 1100 K), and the resulting C_7H_7 radicals largely converts to $C_6H_5C_2H_4C_6H_5$. In contrast, the production of C_7H_7 from toluene pyrolysis occurs at elevated temperatures, so a considerable portion of C_7H_7 dissociates or combines with typical high-temperature species like C_2H_2 and C_3H_3, inhibiting the formation of $C_6H_5C_2H_4C_6H_5$. Besides, at high temperatures the formed $C_6H_5C_2H_4C_6H_5$ decomposes back to C_7H_7, so that the net production of $C_6H_5C_2H_4C_6H_5$ is much lower. Fluorene ($C_{13}H_{10}$) is predominantly produced from the consumption of $C_6H_5CH_2C_6H_5$, so the offset of the concentration profile shows at the temperature where $C_6H_5CH_2C_6H_5$ starts to decompose in each

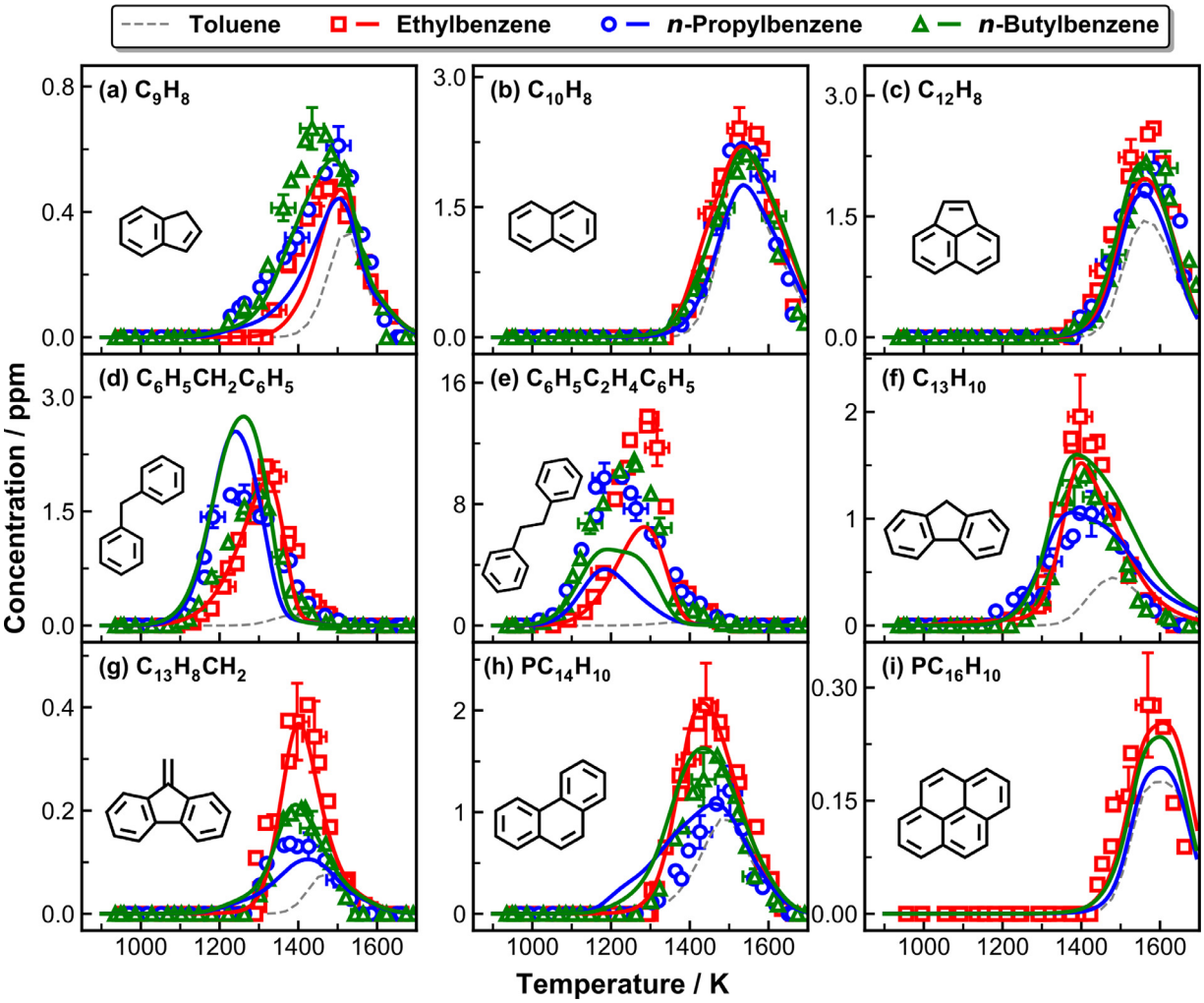

Fig. 11. Experimental (symbols) and simulated (lines) concentrations of PAH products as a function of T_5 in C_8–C_{10} linear alkylbenzenes pyrolysis. Simulated speciation profile in 100 ppm toluene pyrolysis are shown as the dashed lines for comparison purpose.

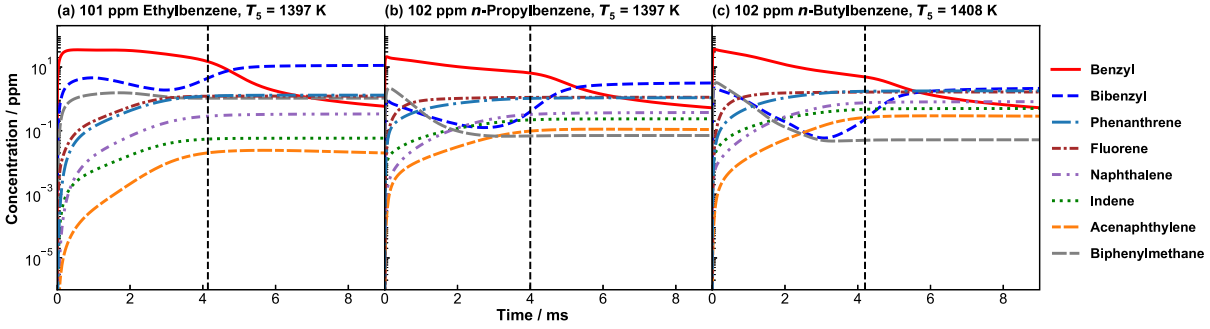

Fig. 12. Simulated time-resolved concentrations of benzyl and major PAH species with measured pressure profiles in the pyrolysis of C_8–C_{10} linear alkylbenzenes at around T_5 = 1400 K. The vertical dashed lines indicate the start of post-shock cooling.

case. Since the consumption phases of the $C_6H_5CH_2C_6H_5$ concentration profiles differ less than the formation phases among the three case, the speciation of $C_{13}H_{10}$ covers a relatively similar temperature window in C_8–C_{10} alkylbenzenes pyrolysis, as can be seen in Fig. 11(f). The peak concentrations of $C_{13}H_{10}$ are in accordance with the levels of $C_6H_5CH_2C_6H_5$ in the three reaction systems.

The formation of indene (C_9H_8) already starts at around 1200 K in the pyrolysis of *n*-propylbenzene and *n*-butylbenzene, much lower than that in the case of ethylbenzene. ROP analysis was performed for C_9H_8 at different temperatures from 1300 to 1450 K, where the C_9H_8 concentrations keep accumulating. The results, shown as percentage contributions by different reactions, are provided in Fig. 14. The formation of C_9H_8 is dominated by the C_2+C_7 reactions over the entire temperature range in the pyrolysis of all three fuels, in particular, by the reaction $C_7H_7+C_2H_2 = C_9H_8+H$. The H atom loss of indanyl radical ($C_9H_9 = C_9H_8+H$) and the reaction $C_7H_5+C_2H_4 = C_9H_8+H$ have more significant contributions in *n*-propylbenzene and *n*-butylbenzene pyrolysis, because of the higher abundance of C_2H_4, which can combine with C_7H_7 to produce indane (C_9H_{10}). Minor contributions from the reaction

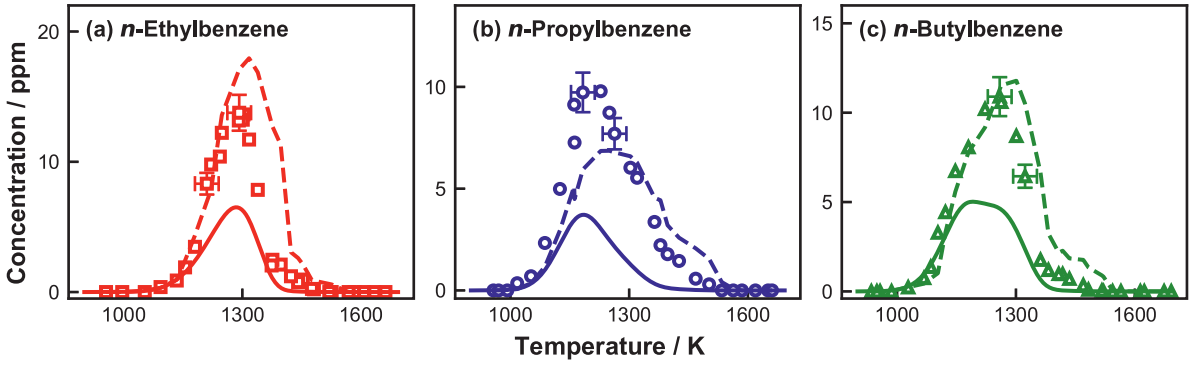

Fig. 13. Bibenzyl ($C_6H_5C_2H_4C_6H_5$) concentrations as a function of T_5 in the pyrolysis of C_8–C_{10} linear alkylbenzenes. Symbols: measurements; Solid lines, simulations with constant pressure of 20 bar and reaction time of 4.0 ms. Dashed lines, simulations with measured pressure profiles up to 10.0 ms.

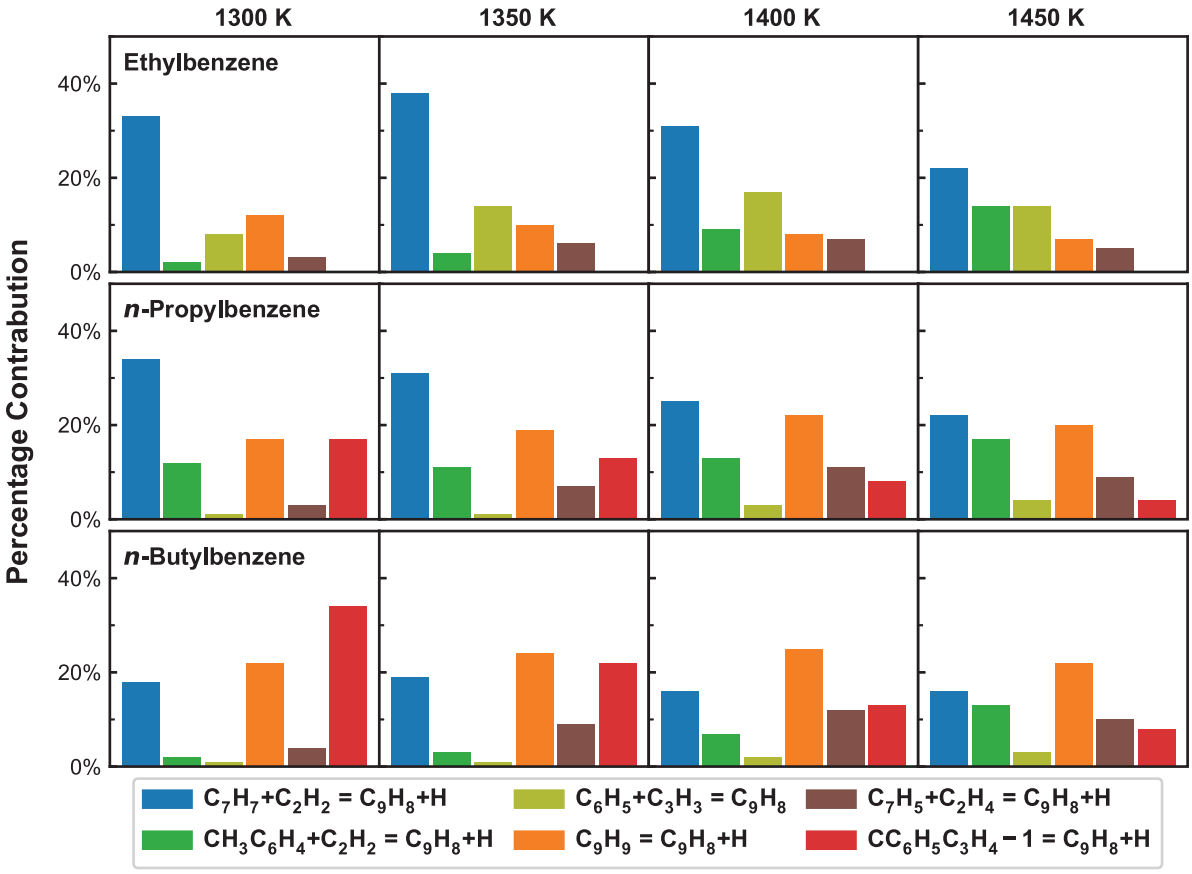

Fig. 14. ROP analysis for the formation of indene (C_9H_8) in C_8–C_{10} linear alkylbenzenes pyrolysis at 1300 K, 1350 K, 1400 K and 1450 K.

$C_3H_3+C_6H_5 = C_9H_8$ can be spotted, whose importance shows an increasing trend when raising the temperature. The reaction $CC_6H_5C_3H_4$–1 = H + C_9H_8, contributes to the formation of C_9H_8 in *n*-propylbenzene and *n*-butylbenzene pyrolysis, and it plays a more important role in the case of *n*-butylbenzene, particularly at lower temperatures. The pathway leading to C_9H_8 through the intermediate $C_6H_5\dot{C}HCH{=}CH_2$ ($CC_6H_5C_3H_4$–1) was mentioned in the kinetic modeling section (see Scheme 1) as a potential fuel-specific PAH formation channel, as C_9H_8 contains the same number of carbon atoms with *n*-propylbenzene. The stronger effects of this pathway in *n*-butylbenzne pyrolysis can be explained by the higher production of the precursor $CC_6H_5C_3H_4$–1. In both cases of *n*-propylbenzene and *n*-butylbenzene, $CC_6H_5C_3H_4$–1 results from the consumption of allylbenzene ($C_6H_5C_3H_5$–1) which is among the initial products of fuel decomposition, as can be seen in Figs. 6 and 7. $C_6H_5C_3H_5$–1 is measured of a peak concentration at around 1 ppm in the pyrolysis of *n*-butylbenzene (see Fig. 9(f)), while only trace quantity (10^{-1} ppm) is detected in the pyrolysis of *n*-propylbenzene, and an accurate quantification is not feasible because the signals of $C_6H_5C_3H_5$–1 and the fuel *n*-propylbenzene are largely overlapped. $C_6H_5C_3H_5$–1 comes from the decomposition of the fuel radical $C_6H_5CH_2\dot{C}HCH_2CH_3$ ($C_6H_5C_4H_8$–C) in *n*-butylbenzene pyrolysis, while in the case of *n*-propylbenzene, the formation channel through the C–H β-scission of $C_6H_5CH_2\dot{C}HCH_3$ ($C_6H_5C_3H_6$-B) is not competitive, since the C_3

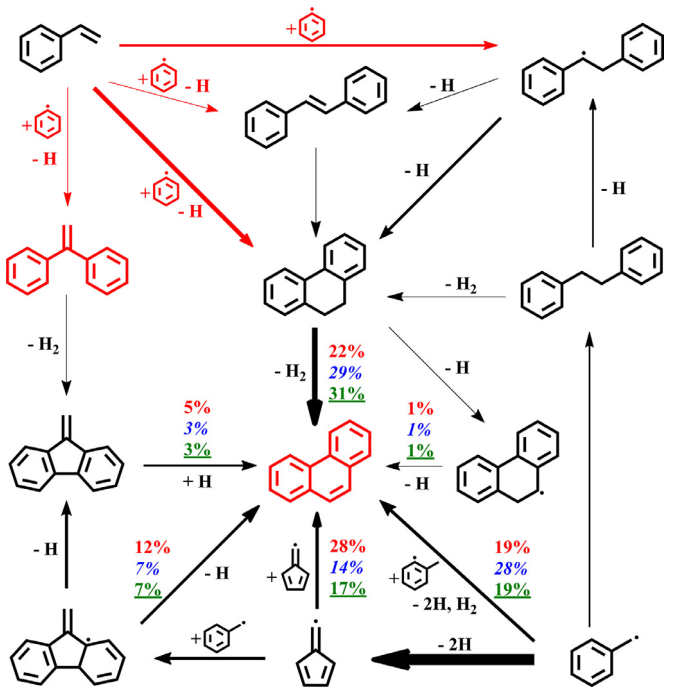

Fig. 15. The reaction pathways leading to phenanthrene formation at T_5 of 1450 K in the pyrolysis of C_8–C_{10} linear alkylbenzenes. The thickness of the arrows represents the carbon flux through the corresponding reactions. The percentage numbers (ethylbenzene: normal; *n*-propylbenzene: *italic;* *n*-butylbenzene: underlined) represent the contributions to the phenanthrene formation by corresponding reactions. The $C_6H_5C_2H_3$+C_6H_5 reaction pathways are highlighted in red. (For interpretation of the references to color in this figure legend, the reader is referred to the web version of this article.)

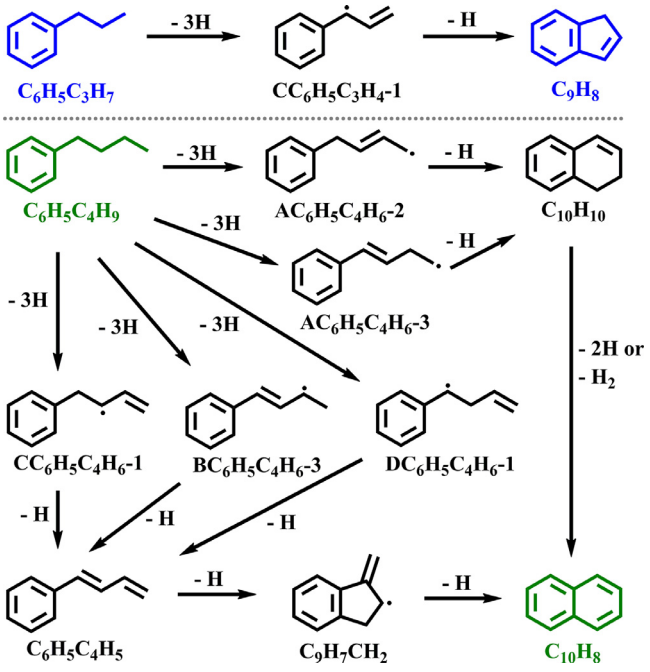

Scheme 1. Schematic for reaction pathways leading to fused PAH species containing the same number of carbon atoms with the fuels.

side chain structure can hardly survive the fuel decay dominated by C–C bond fissions.

When raising the temperature above 1300 K, two $C_{14}H_{10}$ isomers, 9-methylene-fluorene ($C_{13}H_8CH_2$) and phenanthrene ($PC_{14}H_{10}$), appear among the products of C_8–C_{10} linear alkylbenzenes pyrolysis. It is noted that their concentration profiles span over the same temperature range but their peak concentrations differ evidently among the three cases, and such phenomena can be well reproduced by the kinetic model. The reaction pathways leading to $PC_{14}H_{10}$ formation, based on ROP analyses of specific species, at the temperature of 1450 K in the pyrolysis of C_8–C_{10} alkylbenzenes are shown in Fig. 15. The same reactions are responsible for the formation of $PC_{14}H_{10}$ in the three cases, though their relative importance varies slightly. The dehydrogenation of dihydrophenanthrene ($C_{14}H_{12}$) is the largest contributor, and the self-recombination of C_7H_5, the recombination of the C_7H_7+$C_6H_4CH_3$ and the ring-rearrangement of $C_{13}H_9CH_2$ are other important sources. Similar reaction pathways are responsible for the $PC_{14}H_{10}$ formation in toluene pyrolysis, as discussed in [34]. But if only relevant reaction sequences in [34] were considered in the kinetic model, the concentrations of $PC_{14}H_{10}$ in C_8–C_{10} alkylbenzenes pyrolysis would be underestimated by over 40%. The enhanced model performance regarding the predictions for $PC_{14}H_{10}$ concentrations lies in the inclusion of the $C_6H_5C_2H_3$+C_6H_5 reactions mentioned in the kinetic model section, and these pathways are highlighted in red in Fig. 15. In the pyrolysis of C_8–C_{10} alkylbenzenes, because of the abundant $C_6H_5C_2H_3$, $C_{14}H_{12}$ predominantly originates from the addition-elimination reaction $C_6H_5C_2H_3$+C_6H_5 = $C_{14}H_{12}$+H, instead of exclusively forming through the stepwise dehydrogenation and isomerization of $C_6H_5C_2H_4C_6H_5$, as proposed by Sinha and Raj [49], in the case of toluene pyrolysis [34]. The inclusion of $C_6H_5C_2H_3$+C_6H_5 reactions in the kinetic model is further justified by experimental results of styrene pyrolysis under similar conditions. As shown in Fig. S6, the formation of $PC_{14}H_{10}$ starts at the initial stage of styrene decomposition, and the peak concentration approaches 4 ppm. Simulations using the current kinetic model, with and without the $C_6H_5C_2H_3$+C_6H_5 reactions, are both performed and compared to the measurements. The prediction for $PC_{14}H_{10}$ concentration profile is considerably improved and the decomposition reactivity of $C_6H_5C_2H_3$ is better captured when the $C_6H_5C_2H_3$+C_6H_5 reactions are integrated in the kinetic model. The PAH formation kinetics in styrene pyrolysis will be focused on in future studies.

A few of the PAH species only form in high-temperature regimes over 1400 K where the fuels are completely consumed, including naphthalene ($C_{10}H_8$), acenaphthylene ($C_{12}H_8$) and pyrene ($C_{16}H_{10}$), as can be identified from Fig. 11. Scheme 1 shows that fuel-related reactions, which are expected to contribute to the formation of PAH species with the same carbon numbers as the fuels, involve those from the C_{10} intermediates produced in *n*-butylbenzene pyrolysis to $C_{10}H_8$. Though being taken into consideration in the kinetic model construction, the effects of such reactions have minimal impacts on the formation of $C_{10}H_8$. The $C_{10}H_8$ concentration profiles in the pyrolysis of C_8–C_{10} alkylbenzenes as well as toluene share the same temperature window and comparable peak values. A similar $C_{10}H_8$ formation pattern is found in all cases: it is governed by the reaction C_7H_5+C_3H_3 = $C_{10}H_8$, and the ring-rearrangement of $C_9H_7CH_2$ formed through the recombination reactions of C_3H_3+C_7H_7 and CH_3+C_9H_7, as addressed in [34]. An analogous phenomenon that the speciation temperature window is not altered by the side chain lengths of the fuel is also seen in the concentration profiles of acenaphthylene ($C_{12}H_8$) which is formed via the recombination of C_3H_3+C_9H_7 [43] in the pyrolysis of all fuels. In comparison to that in toluene pyrolysis, the slightly higher $C_{12}H_8$ peak concentrations in the cases of C_8–C_{10} alkylbenzenes are due to the larger production C_9H_7 and C_3H_3. Pyrene ($PC_{16}H_{10}$) is also deemed to be among the PAH products which are not significantly affected by the fuel side chain lengths, though only the measured concentration profile in ethylbenzene pyrolysis is presented in Fig. 11(i). Those in

n-propylbenzene and *n*-butylbenzene pyrolysis are scattered, due to a deteriorating signal/noise ratio when species concentrations approach the detection limit of 0.1 ppm. $C_{16}H_{10}$ concentration profiles, including the measured one in ethylbenzene pyrolysis and the simulations in separate cases, cover the same temperature range and have similar peaks. The current kinetic model can well predict the $PC_{16}H_{10}$ concentration measurements in ethylbenzene pyrolysis, while for those in *n*-propylbenzene and *n*-butylbenzene, the model verification still requires further experiments with larger fuel contents consequently yielding higher $PC_{16}H_{10}$ concentrations.

5. Conclusions

In this work, pyrolysis experiments of C_8–C_{10} linear alkylbenzenes were carried out in a single-pulse shock tube over a temperature range of 950–1700 K at around 20 bar under highly argon-diluted conditions. Species concentrations were measured as a function of the temperature in each experimental set. A kinetic model was proposed, which can well reproduce the fuel decomposition reactivity and the speciation behaviors in individual reaction systems. Comparisons regarding the fuel decomposition reactivity, the contents of specific intermediates (small acyclic intermediates, monocyclic and polycyclic aromatic hydrocarbons), as well as the responsible reaction schemes among the three cases, were made by combining the quantitative measurements and modeling analyses. All the three fuels have remarkably higher decomposition reactivity than toluene, the simplest alkylbenzene. With the lengthening of the side chain, *n*-propylbenzene decomposes evidently faster than ethylbenzene, and at an almost identical pace with *n*-butylbenzene decomposition. The higher-than-expected decomposition reactivity of *n*-propylbenzene arises from a higher production of H atoms in the initial fuel decomposition steps, which also leads to larger amounts of benzene compared to the other two cases. The consumption of all three fuels are dominated by the benzylic C–C fissions, so the PAH formation pathways starting from benzyl radicals prevail the PAH speciation in the three cases, similar to the case of toluene pyrolysis. A large extent of similarity exists in PAH speciation profiles in the three reaction systems, with regards to both temperature windows and the peak concentrations, particularly for the PAH species produced at high temperatures. Fuel-specific reaction pathways contribute to the formation of indene in *n*-butylbenzene and *n*-propylbenzene pyrolysis at relatively low temperatures. Styrene is of high abundance in the pyrolysis of C_8–C_{10} linear alkylbenzenes. Consequently, the addition-elimination reaction between styrene and phenyl leading to dihydrophenanthrene is identified as an important channel of phenanthrene formation.

Declaration of Competing Interest

The authors declare that they have no known competing financial interests or personal relationships that could have appeared to influence the work reported in this paper.

Acknowledgments

This project has received funding from the European Research Council (ERC) under the European Union's Horizon 2020 research and innovation program (grant agreement No. 756785).

Supplementary materials

Supplementary material associated with this article can be found, in the online version, at doi:10.1016/j.combustflame.2020.07.031.

References

[1] S.M. Sarathy, A. Farooq, G.T. Kalghatgi, Recent progress in gasoline surrogate fuels, Prog. Energy Combust. 65 (2018) 67–108.
[2] W.J. Pitz, C.J. Mueller, Recent progress in the development of diesel surrogate fuels, Prog. Energy Combust. 37 (2011) 330–350.
[3] P. Dagaut, M. Cathonnet, The ignition, oxidation, and combustion of kerosene: a review of experimental and kinetic modeling, Prog. Energy Combust. 32 (2006) 48–92.
[4] H.-P.S. Shen, M.A. Oehlschlaeger, The autoignition of C8H10 aromatics at moderate temperatures and elevated pressures, Combust. Flame 156 (2009) 1053–1062.
[5] D. Darcy, C.J. Tobin, K. Yasunaga, J.M. Simmie, J. Würmel, W.K. Metcalfe, T. Niass, S.S. Ahmed, C.K. Westbrook, H.J. Curran, A high pressure shock tube study of n-propylbenzene oxidation and its comparison with n-butylbenzene, Combust. Flame 159 (2012) 2219–2232.
[6] D. Darcy, H. Nakamura, C.J. Tobin, M. Mehl, W.K. Metcalfe, W.J. Pitz, C.K. Westbrook, H.J. Curran, A high-pressure rapid compression machine study of n-propylbenzene ignition, Combust. Flame 161 (2014) 65–74.
[7] X. Hui, A.K. Das, K. Kumar, C.-J. Sung, S. Dooley, F.L. Dryer, Laminar flame speeds and extinction stretch rates of selected aromatic hydrocarbons, Fuel 97 (2012) 695–702.
[8] C. Ji, E. Dames, H. Wang, F.N. Egolfopoulos, Propagation and extinction of benzene and alkylated benzene flames, Combust. Flame 159 (2012) 1070–1081.
[9] X. Hui, C.-J. Sung, Laminar flame speeds of transportation-relevant hydrocarbons and jet fuels at elevated temperatures and pressures, Fuel 109 (2013) 191–200.
[10] A. Comandini, T. Dubois, N. Chaumeix, Laminar flame speeds of n-decane, n-butylbenzene, and n-propylcyclohexane mixtures, Proc. Combust. Inst. 35 (2015) 671–678.
[11] M. Mehl, O. Herbinet, P. Dirrenberger, R. Bounaceur, P.-.A. Glaude, F. Battin-Leclerc, W.J. Pitz, Experimental and modeling study of burning velocities for alkyl aromatic components relevant to diesel fuels, Proc. Combust. Inst. 35 (2015) 341–348.
[12] M. Szwarc, The C–C bond energy in ethylbenzene, J. Chem. Phys. 17 (1949) 431–435.
[13] C. Leigh, M. Szwarc, The pyrolysis of n-propyl-benzene and the heat of formation of ethyl radical, J. Chem. Phys. 20 (1952) 403–406.
[14] G. Esteban, J. Kerr, A. Trotman-Dickenson, Pyrolysis of ethyl-, n-propyl-, and n-butyl-benzene and the heats of formation of the benzyl and n-propyl radicals, J. Chem. Soc. (1963) 3873–3879.
[15] W. Clark, S. Price, Free-radical and molecular processes in the pyrolysis of ethylbenzene, Can. J. Chem. 48 (1970) 1059–1064.
[16] D.A. Robaugh, S.E. Stein, Very-low-pressure pyrolysis of ethylbenzene, isopropylbenzene, and tert-butylbenzene, Int. J. Chem. Kinet. 13 (1981) 445–462.
[17] L. Mizerka, J. Kiefer, The high temperature pyrolysis of ethylbenzene: evidence for dissociation to benzyl and methyl radicals, Int. J. Chem. Kinet. 18 (1986) 363–378.
[18] W. Müller-Markgraf, J. Troe, Thermal decomposition of ethylbenzene, styrene, and bromophenylethane: UV absorption study in shock waves, J. Phys. Chem. 92 (1988) 4914–4922.
[19] U. Brand, H. Hippler, L. Lindemann, J. Troe, Carbon-carbon and carbon-hydrogen bond splits of laser-excited aromatic molecules. 1. Specific and thermally averaged rate constants, J. Phys. Chem. 94 (1990) 6305–6316.
[20] W. Yuan, Y. Li, G. Pengloan, C. Togbé, P. Dagaut, F. Qi, A comprehensive experimental and kinetic modeling study of ethylbenzene combustion, Combust. Flame 166 (2016) 255–265.
[21] W. Yuan, Y. Li, P. Dagaut, Y. Wang, Z. Wang, F. Qi, A comprehensive experimental and kinetic modeling study of n-propylbenzene combustion, Combust. Flame 186 (2017) 178–192.
[22] Y. Zhang, C. Cao, Y. Li, W. Yuan, X. Yang, J. Yang, F. Qi, T.-.P. Huang, Y.-.Y. Lee, Pyrolysis of n-butylbenzene at various pressures: influence of long side-chain structure on alkylbenzene pyrolysis, Energy Fuel 31 (2017) 14270–14279.
[23] Y. Li, J. Cai, L. Zhang, J. Yang, Z. Wang, F. Qi, Experimental and modeling investigation on premixed ethylbenzene flames at low pressure, Proc. Combust. Inst. 33 (2011) 617–624.
[24] Z. Wang, Y. Li, F. Zhang, L. Zhang, W. Yuan, Y. Wang, F. Qi, An experimental and kinetic modeling investigation on a rich premixed n-propylbenzene flame at low pressure, Proc. Combust. Inst. 34 (2013) 1785–1793.
[25] W. Yuan, Y. Li, Z. Wang, Y. Wang, L. Zhao, Y. Zhang, Z. Zhou, F. Qi, Experimental and kinetic modeling study of premixed n-butylbenzene flames, Proc. Combust. Inst. 36 (2017) 815–823.
[26] P. Dagaut, A. Ristori, A. El Bakali, M. Cathonnet, Experimental and kinetic modeling study of the oxidation of n-propylbenzene, Fuel 81 (2002) 173–184.
[27] P. Diévart, P. Dagaut, The oxidation of n-butylbenzene: experimental study in a JSR at 10 atm and detailed chemical kinetic modeling, Proc. Combust. Inst. 33 (2011) 209–216.
[28] B. Husson, R. Bounaceur, K. Tanaka, M. Ferrari, O. Herbinet, P.A. Glaude, R. Fournet, F. Battin-Leclerc, M. Crochet, G. Vanhove, Experimental and modeling study of the oxidation of n-butylbenzene, Combust. Flame 159 (2012) 1399–1416.
[29] B. Husson, M. Ferrari, O. Herbinet, S.S. Ahmed, P.-.A. Glaude, F. Battin-Leclerc, New experimental evidence and modeling study of the ethylbenzene oxidation, Proc. Combust. Inst. 34 (2013) 325–333.
[30] R. Robinson, R. Lindstedt, A comparative ab initio study of hydrogen abstraction from n-propyl benzene, Combust. Flame 160 (2013) 2642–2653.

[31] L. Ye, L. Xing, W. Yuan, Y. Li, L. Zhang, F. Qi, Predictive kinetics on the formation and decomposition of ethylbenzene, Proc. Combust. Inst. 36 (2017) 533–542.
[32] S. Gudiyella, K. Brezinsky, High pressure study of n-propylbenzene oxidation, Combust. Flame 159 (2012) 940–958.
[33] S. Gudiyella, K. Brezinsky, The high pressure study of n-propylbenzene pyrolysis, Proc. Combust. Inst. 34 (2013) 1767–1774.
[34] W. Sun, A. Hamadi, S. Abid, N. Chaumeix, A. Comandini, Probing PAH formation chemical kinetics from benzene and toluene pyrolysis in a single-pulse shock tube, Proc. Combust. Inst. 38 (2020), doi:10.1016/j.proci.2020.06.077.
[35] W. Sun, A. Hamadi, S. Abid, N. Chaumeix, A. Comandini, An experimental and kinetic modeling study of phenylacetylene decomposition and the reactions with acetylene/ethylene under shock tube pyrolysis conditions, Combust. Flame 220 (2020) 257–271.
[36] H. Wang, R. Xu, K. Wang, C.T. Bowman, R.K. Hanson, D.F. Davidson, K. Brezinsky, F.N. Egolfopoulos, A physics-based approach to modeling real-fuel combustion chemistry-I. Evidence from experiments, and thermodynamic, chemical kinetic and statistical considerations, Combust. Flame 193 (2018) 502–519.
[37] R. Tranter, R. Sivaramakrishnan, N. Srinivasan, K. Brezinsky, Calibration of reaction temperatures in a very high pressure shock tube using chemical thermometers, Int. J. Chem. Kinet. 33 (2001) 722–731.
[38] W. Tsang, C.M. Rosado-Reyes, Unimolecular rate expression for cyclohexene decomposition and its use in chemical thermometry under shock tube conditions, J. Phys. Chem. A 119 (2015) 7155–7162.
[39] X. Han, J.M. Mehta, K. Brezinsky, Temperature approximations in chemical kinetics studies using single pulse shock tubes, Combust. Flame 209 (2019) 1–12.
[40] A. Matsugi, A. Miyoshi, Modeling of two-and three-ring aromatics formation in the pyrolysis of toluene, Proc. Combust. Inst. 34 (2013) 269–277.
[41] I. Tokmakov, M. Lin, Combined quantum chemical/RRKM-ME computational study of the phenyl+ ethylene, vinyl+ benzene, and H+ styrene reactions, J. Phys. Chem. A 108 (2004) 9697–9714.
[42] W. Pejpichestakul, E. Ranzi, M. Pelucchi, A. Frassoldati, A. Cuoci, A. Parente, T. Faravelli, Examination of a soot model in premixed laminar flames at fuel-rich conditions, Proc. Combust. Inst. 37 (2019) 1013–1021.
[43] H. Jin, L. Xing, J. Hao, J. Yang, Y. Zhang, C. Cao, Y. Pan, A. Farooq, A chemical kinetic modeling study of indene pyrolysis, Combust. Flame 206 (2019) 1–20.
[44] COSILAB, The combustion simulation laboratory, Rotexo GmbH & Co., KG, Haan, Germany, 2009 Version 3.3.2.
[45] W. Tang, K. Brezinsky, Chemical kinetic simulations behind reflected shock waves, Int. J. Chem. Kinet. 38 (2006) 75–97.
[46] Y.-R. Luo, Handbook of bond dissociation energies in organic compounds, CRC Press, 2002.
[47] N. Hansen, X. He, R. Griggs, K. Moshammer, Knowledge generation through data research: new validation targets for the refinement of kinetic mechanisms, Proc. Combust. Inst. 37 (2019) 743–750.
[48] L.A. Mertens, I.A. Awan, D.A. Sheen, J.A. Manion, Evaluated site-specific rate constants for reaction of isobutane with H and CH3: shock tube experiments combined with bayesian model optimization, J. Phys. Chem. A 122 (2018) 9518–9541.
[49] S. Sinha, A. Raj, Polycyclic aromatic hydrocarbon (PAH) formation from benzyl radicals: a reaction kinetics study, Phys. Chem. Chem. Phys. 18 (2016) 8120–8131.